Experimental Demonstration of Single Mode-Splitting in Microring With Bragg Gratings

Qiangsheng Huang, Keqi Ma, and Sailing He, *Fellow, IEEE*

***Abstract*— We demonstrate single mode-splitting in two types of microring resonators with Bragg gratings. In the first device type, gratings are periodically embedded to the inner wall of the microring resonator. By adjusting the reflection coefficient of the grating and the self-coupling coefficient between the waveguide and microring, experimental results show that the distance between the splitting dips can vary from 0 to more than 1 nm. In the second device type, Bragg gratings break into two identical parts with a π phase shift between them. The center peak in the mode-splitting spectrum has a full-width at half-maximum of 0.1 nm. The spectra can also be a Fano-type transmission, when the phase shift deviates from π.**

***Index Terms*— Optical mode splitting, optical resonators, Bragg gratings, silicon photonics.**

I. INTRODUCTION

MODE-SPLITTING in coupled resonator systems has gained increasing interesting for their special properties such as electromagnetically-induced-transparency (EIT) transmission [1], Fano-type transmission [2], fast and slow light effects [3], etc. Mode-splitting can be achieved with coupled ring resonators [4], two mutually coupled microspheres [5], and other devices. However, the device should carefully align with the resonant wavelength. A different mode-splitting method, which involves coupling between forward- and backward-propagating modes of an optical resonator, has also been exploited [6]–[11]. The phases in the two counter-propagating modes are inherently matched. This has been used for single nanoparticle detection with self-referenced detection [7], high order optical filters [8], and dense wavelength conversion [9]. Through inserting distributed Bragg gratings (DBRs) or π-shifted DBRs in fiber ring resonator, the strain sensors have been experimentally demonstrated [10], [11]. However, in these structures, by inserting partial or DBRs in ring resonators, the mode-splitting will appear in all resonance wavelengths. In this way, as an optical filter, the FSR of such a microring cannot serve as a single or dual wavelength filter. As a sensor, based on measuring the distance of the splitting peaks or tracing the position of the resonance wavelength, the FSR of the microring resonators will limit its measurement range. One way to solve this problem is to find a resonance structure that has single mode-splitting spectrum, without FSR.

Recently, two ways to achieve single mode-splitting have been theoretically studied [12]. The first way is to embed the DBRs into half of or an entire microring resonator (MRR). In this DBR-MRR type, the angular period of the DBRs is equal to half of the angular period of the resonance order, so the DBRs will couple with only one resonance mode. This DBR-MRR type can also be used for a single wavelength mirror [13], an orbital angular momentum emitter [14] and RI optical sensor [15]. The second way to achieve single mode-splitting is to cover the MRR with π-shifted DBRs, through breaking the previous DBRs in two sections and introducing a π-shift between them. Even though some theoretical study has predicted that the single-mode splitting will appear in DBR-MRR [12], [15] or π-shifted DBR-MRR [12], [16], there is still a lack of experimental demonstration.

In this letter, we present design, fabrication and experimental results for these two types of single mode-splitting structures based on silicon-on-insulator (SOI) technology. In Section II, we experimentally show the influence of the reflectivity coefficient and self-coupling coefficient on the mode-splitting of the DBR-MRR. In Section III, we experimentally demonstrate single mode-splitting in the π-shifted DBR-MRR with narrowband and Fano-type transmission spectra. These devices are fabrications of SOI, allowing dense integration with other silicon photonic devices.

II. SINGLE MODE-SPLITTING IN THE DBR-MRR

Fig. 1 (a) shows the schematic of the DBR-MRR, with DBRs embedded in the inner wall of the entire MRR. The transmission spectra of the device can be analyzed by the transmission matrix method [12], [17]. A_i (or B_i) gives steady-state amplitudes of the forward (or backward) mode at different periods. Λ is the period of grating, l_g is the width of the grating teeth, h_g is the height of the grating teeth, D (defined as l_g/Λ) is the duty cycle of the grating, r is

Manuscript received January 12, 2015; revised March 16, 2015; accepted April 6, 2015. Date of publication April 20, 2015; date of current version June 9, 2015. This work was supported in part by the 863 project under Grant 2012AA012201, in part by NSFC projects under Grant 91233208, in part by the Science and Technology Department of Zhejiang Province under Grant 2010R50007, in part by the Fundamental Research Funds for the Central Universities, in part by Swedish VR Grant (621-2011-4620), and in part by AOARD.

Q. Huang and K. Ma are with the Zhejiang Provincial Key Laboratory for Sensing Technologies, Centre for Optical and Electromagnetic Research, Sino-Sweden Joint Research Center of Photonics, Zhejiang University, Hangzhou 310058, China.

S. He is with the Zhejiang Provincial Key Laboratory for Sensing Technologies, Centre for Optical and Electromagnetic Research, Sino-Sweden Joint Research Center of Photonics, Zhejiang University, Hangzhou 310058, China, and also with the Department of Electromagnetic Engineering, Royal Institute of Technology, Stockholm 100 44, Sweden (e-mail: sailing@jorcep.org).

Color versions of one or more of the figures in this letter are available online at http://ieeexplore.ieee.org.

Digital Object Identifier 10.1109/LPT.2015.2422731

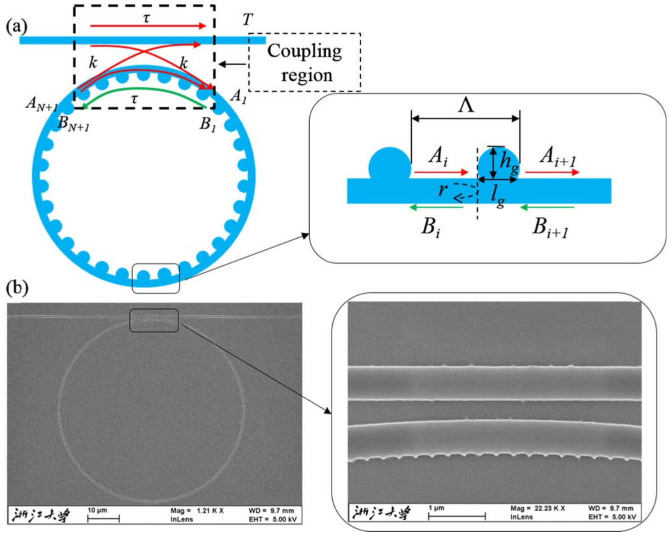

Fig. 1. (a) The schematic of the DBR-MRR. Bragg gratings are embedded on the inner wall of the entire microring resonator. (b) Scanning Electron Microscopy (SEM) image of the fabricated device.

the reflection coefficient from a waveguide to a waveguide with grating tooth, κ is the coupling magnitude between the DBR-MRR and the bus waveguide. τ is the self-coupling coefficient, defined as $(1-\kappa^2)^{1/2}$.

When the number of the DBRs (N) is equal to twice the order of the resonant modes (m), namely $N = 2m$, the mth order resonant mode in the microring will be located in the middle of stop band simultaneously. The back-propagation mode will be excited and there will be two counter-propagation modes coupled to each other and induce two split resonances. The splitting wavelengths are "symmetric" and "anti-symmetric" resonant wavelength located in the band edges of the Bragg gratings [15]. Because wavelengths at other orders of the resonant modes will not be influenced by the DBRs, we can achieve single mode-splitting in the mth order resonant mode.

The device is fabricated on a silicon-on-insulator wafer with a top silicon layer thickness of 220nm and silica buffer thickness of 2μm. The DBR-MRR and focusing grating coupler pattern, used for coupling the light from the fiber to the silicon waveguide, are defined by electron beam lithography with negative resist ma-N 2403. Then we use reactive ion plasma etching to transfer the pattern to a silicon layer. The etching depth is about 85nm. After fabrication, the device is covered by a 300nm thick PMMA. The SEM of the device before coating the PMMA is shown in Fig. 1(b). The cross-section of the DBR-MRR is a shallow etch waveguide with 600nm (wide) by 85nm (ridge height). Measurement is performed by coupling TE-polarized light from a tunable laser to the focus grating coupler through a polarizer.

Fig. 2(a) shows the measured normalized transmission spectrum for a DBR-MRR with a 30μm radius. The N is 658. The calculated FSR for a 30μm radius microring with the same waveguide structure is about 3.3nm. However,

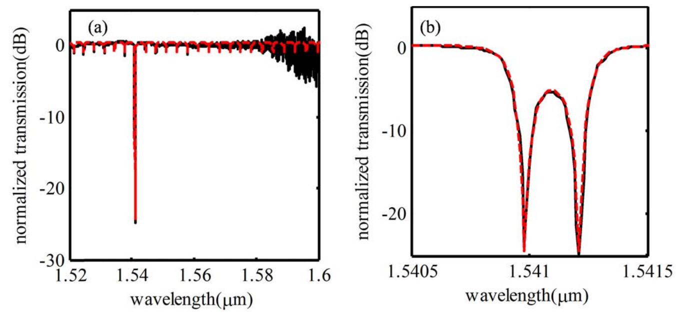

Fig. 2. (a) Measured normalized transmission spectra for the DBR-MRR. (b) Enlarged view of the measured spectra around the mode-splitting dip. The solid black lines are measured results and the dashed red lines are theoretical fits.

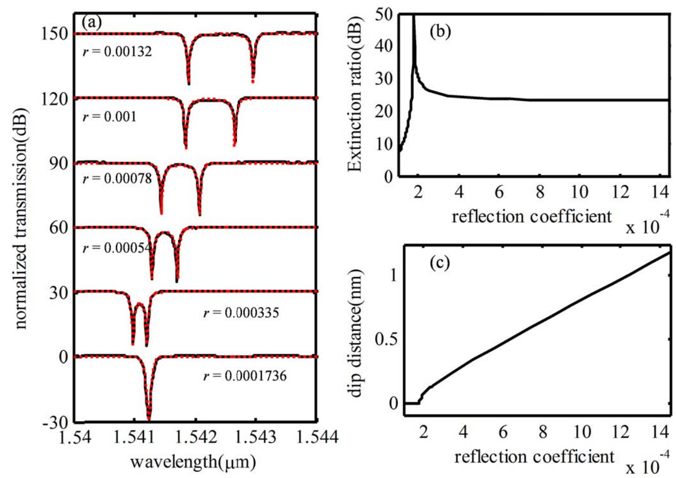

Fig. 3. (a) Experimental normalized transmission spectra (black, solid line) and theoretical fits (red, dashed line) for the DBR-MRR with different r. (b, c) Theoretically predicted extinction ratio and dip distance of DBR-MRR with varying r.

we can see that from 1520nm to 1600nm, which is limited by the tunable laser scanning range, there only exists single mode-splitting. The noise above 1580nm is caused by the low coupling efficiency of the focus grating coupler. The dashed red lines in Fig. 2 indicate theoretical fits, which agree well with the experimental results. D (0.2) is measured from the SEM image. The resonant wavelength (1541.1nm) is found from the experimental results. The intrinsic quality factor Q (100,000), τ (0.87), and r (0.000335) are adjusted to fit the spectra of the DBR-MRR.

Fig. 3(a) shows the DBR-MRR with the same τ (0.87) and a different r by changing h_g from 30nm to 80nm in the mask. According to the fitting results, the r varies from the 0.0001736 to 0.00132. The shifts in the resonant wavelengths are caused by fabrication imperfections. We can see that for small r, the mode-splitting degenerates and becomes a single wavelength filter [13]. However, above a critical r_c [12], the mode-splitting distance increases to more than 1nm.

We also sweep the r in order to analyze its effect on the extinction of dips and the distance between the two dips in Fig. 3(b,c). From Fig. 3(b), we can see that the extinction ratio of the dips reaches the maximum point at r_c.

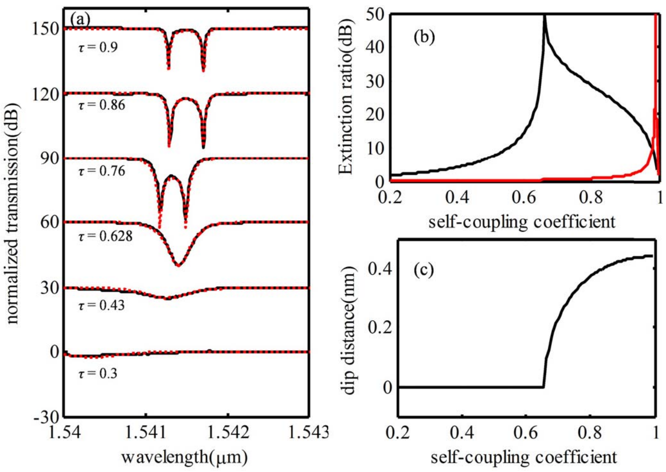

Fig. 4. (a) Experimental normalized transmission spectra (black, solid line) and theoretical fits (red, dashed line) for the DBR-MRR with different τ. (b) Theoretically predicted extinction ratio of DBR-MRR (black, solid line) and MRR (red, dashed line). (c) Theoretically predicted dip distance of DBR-MRR with varying by τ.

Then it becomes saturated with r increasing. From Fig. 3(c) we can see that the distance between two peaks above r_c is proportional to r. The reason is that the two peaks are located in the band edges of the Bragg gratings and the distance of the band edges is proportional to r [15].

We keep r (0.00054) as a constant and sweep τ in Fig. 4. Fig. 4(a) shows the measured transmission spectra and theoretical fits. The distance between the bus waveguide and DBR-MRR varies from 50nm to 300nm. According to the fitting results, the corresponding τ varies from 0.3 to 0.9, N is 658, Q is 100000, D is 0.2. Fig 4(b) shows the extinction ratio of the dips. We can see that after τ reaches the critical τ_c, the extinction ratio decreases from the maximum point. For contrast, the relation between the extinction ratio and τ for a general MRR with the same Q is shown in Fig. 4(b). The large extinction ratio only exists in a narrow τ region, compared to the DBR-MRR region. Fig. 4(c) shows that the distance between the two dips are saturated when τ approaches to 1. By comparing Fig. 3(c) and Fig. 4(c), we find that r determines the maximum mode-splitting distance when τ varies from 0 to 1. By comparing Fig. 3(b) and Fig. 4(b), we find that τ determines the saturation extinction ratio when r is larger than r_c.

III. Single Mode-Splitting in the π-Shifted DBR-MRR

The full theoretical description of the π-shifted DBR-MRR can be found in [12] and [15]. The mode splitting in π-shifted DBR-MRR is caused by the coupling between the defect mode in the π-shifted DBR and the resonance mode in the MRR, which is different from the unshifted DBR-MRR [15]. Fig. 5 (a) shows the schematic of the π-shifted DBR-MRR, through separating the DBRs into two identical sections by inserting a Λ length (π phase-shifted) defect between them. The fabrication material and procedure are the same as that of the unshifted DBR-MRR. However, the etching depth is about 75nm, due to the unstable etching process. In order to increase the reflectivity of the DBRs, the device is not

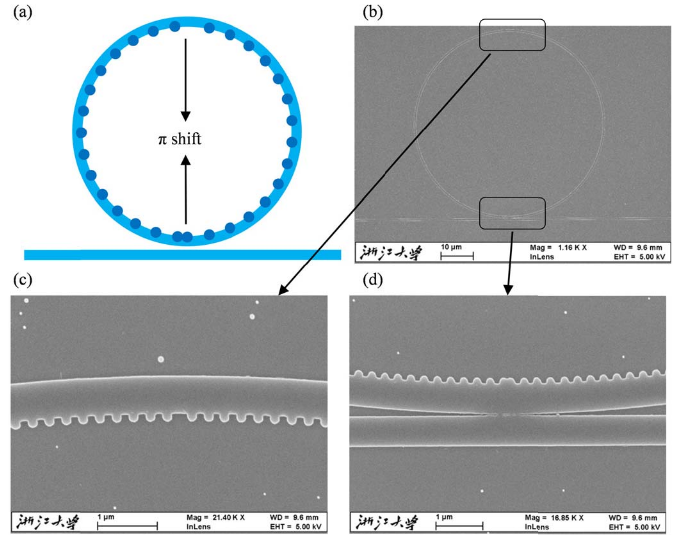

Fig. 5. (a) The schematic of the π-shifted DBR-MRR. There is a defect length Λ in the DBRs. (b) SEM image of the fabricated device. (c, d) Expanded view of the DBR defects in the top and bottom of the MRR.

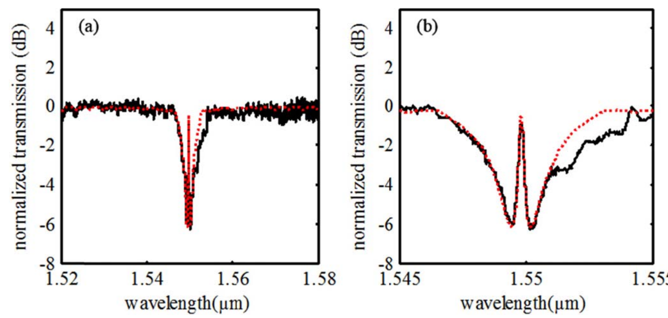

Fig. 6. (a) Measured normalized transmission spectra for a π-shifted DBR-MRR. (b) Enlarged view of the measured spectra around the peak. The solid black lines are the measured results, and the dashed red lines are theoretical fits.

covered by a 300nm thick PMMA. SEMs of the device are shown in Fig. 5(b-d). The cross-section of the DBR-MRR is a shallow etch waveguide with a width of 630nm and ridge height of 75nm. h_g is 120nm.

Fig. 6 shows the measured normalized transmission spectrum for the π-shifted DBR-MRR with a 30μm radius, N of 658, and FSR of 3.3nm. We can see that from 1520nm to 1580nm, which is limited by the bandwidth of the focus grating coupler, there only exists single mode-splitting, which is the same as that of the unshifted DBR-MRR. However, the shape of the mode-splitting spectra is different from the unshifted DBR-MRR devices. The FWHM of the center peak is about 0.2 nm. The dashed red lines in Fig. 6 indicates theoretical fits, which agree well with the experimental results. D (0.6) is measured from the SEM image. The resonant wavelength (1549.8nm) is found from the experimental results. Q (100,000), τ (0.4), and r (0.002) are adjusted to fit the spectra.

In order to reduce the FWHM of the center peak, we increase the reflectivity of the DBRs, through embedding the grating outside of the MRR, presented in Fig. 7. This device has the same structural parameters as the π-shifted interior-DBR-MRR, except that h_g is 100nm, the defect position

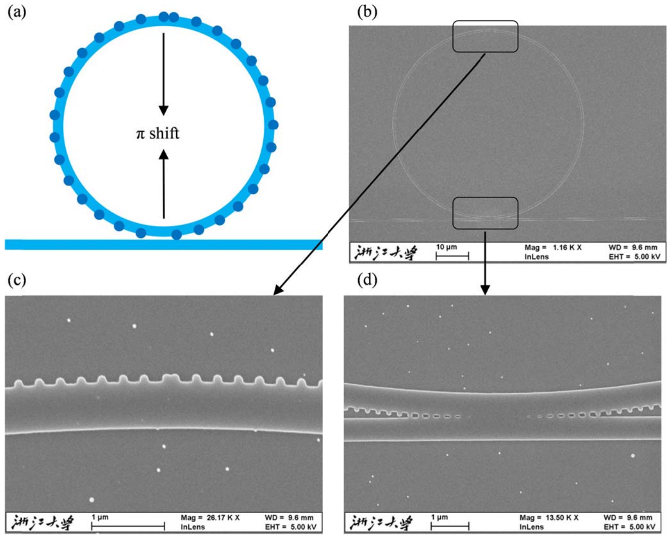

Fig. 7. (a) Schematic of the π-shifted exterior-DBR-MRR, with DBRs embedded outside the MRR. (b) SEM image of the fabricated device. (c, d) Zoomed-in view of the DBR defects on the top and bottom of MRR.

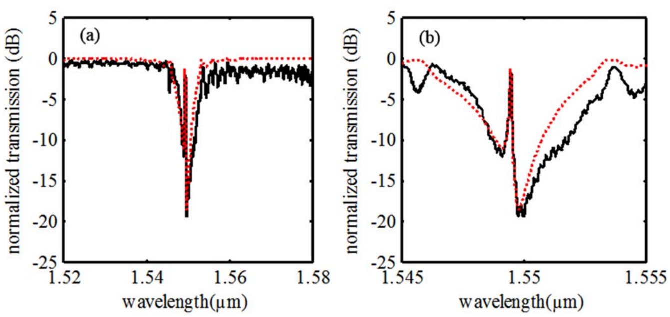

Fig. 8. (a) Measured normalized transmission spectra for the π-shifted exterior-DBR-MRR. (b) Enlarged view of the measured spectra around the Fano-type peak. The solid black lines are measured results and the dashed red lines are theoretical fits.

is opposite to DBR-MRR, and the τ is different due to the gap between the bus waveguide and the altered MRR (shown in Fig. 7(c)).

Fig. 8 shows the measured normalized transmission spectrum for the π-shifted exterior-DBR-MRR. The FWHM of the center peak is reduced to 0.1nm. Due to the imperfect fabrication in Fig. 7 (c), the defect length deviates a little from Λ, which makes the wavelength of the defect mode in the π-shifted DBR different from the resonance wavelength in the MRR. Thus the peak line-shape becomes a Fano-type shape. According to the fitting results, the phase shifts in the defect position is 0.98π. Other fittings parameters are D (0.3), Q (100,000), τ (0.3), and r (0.004). The FWHM can be further reduced by using deep etch DBRs, to increase the reflectivity of the DBRs [12].

IV. Conclusion

We presented design, fabrication and experimental results for single mode-splitting in a DBR-MRR and π-shifted DBR-MRR based on a SOI platform. The transmission matrix method [12], [17] agreed well with the experimental results. For the unshifted DBR-MRR, we experimentally demonstrated that both τ and r had an effect on the extinction ratio and the distance of the dips. The dip distance was changed from 0 to more than 1nm by adjusting r. The r determines the maximum dip distance when τ varies from 0 to 1. However, τ determines the saturation extinction ratio when r is larger than r_c. We also experimentally demonstrated narrowband and Fano-type transmission spectra in the π-shifted DBR-MRR. The FWHM was 0.1nm and it can be further reduced by increasing the reflectivity of the DBRs. We hope that the SOI-based single mode-splitting device can be used to compose filters and sensitive sensors and other compact optical components in silicon photonic devices.

Acknowledgment

The authors thank Yingchen Wu for valuable discussions.

References

[1] X. Yang, M. Yu, D.-L. Kwong, and C. W. Wong, "All-optical analog to electromagnetically induced transparency in multiple coupled photonic crystal cavities," *Phys. Rev. Lett.*, vol. 102, p. 173902, Apr. 2009.

[2] S. Fan, W. Suh, and J. D. Joannopoulos, "Temporal coupled-mode theory for the Fano resonance in optical resonators," *J. Opt. Soc. Amer. A*, vol. 20, no. 3, pp. 569–572, Mar. 2003.

[3] C. Ciminelli, C. E. Campanella, F. Dell'Olio, and M. N. Armenise, "Fast light generation through velocity manipulation in two vertically-stacked ring resonators," *Opt. Exp.*, vol. 18, no. 3, pp. 2973–2986, Feb. 2010.

[4] Q. Xu, S. Sandhu, M. L. Povinelli, J. Shakya, S. Fan, and M. Lipson, "Experimental realization of an on-chip all-optical analogue to electromagnetically induced transparency," *Phys. Rev. Lett.*, vol. 96, p. 123901, Mar. 2006.

[5] A. Naweed, G. Farca, S. I. Shopova, and A. T. Rosenberger, "Induced transparency and absorption in coupled whispering-gallery microresonators," *Phys. Rev. A*, vol. 71, p. 043804, Apr. 2005.

[6] B. E. Little, J.-P. Laine, and S. T. Chu, "Surface-roughness-induced contradirectional coupling in ring and disk resonators," *Opt. Lett.*, vol. 22, no. 1, pp. 4–6, Jan. 1997.

[7] J. Zhu *et al.*, "On-chip single nanoparticle detection and sizing by mode splitting in an ultrahigh-Q microresonator," *Nature Photon.*, vol. 4, pp. 46–49, Jan. 2010.

[8] C. Alonso-Ramos, F. Morichetti, A. Ortega-Moñux, I. Molina-Fernández, M. J. Strain, and A. Melloni, "Dual-mode coupled-resonator integrated optical filters," *IEEE Photon. Technol. Lett.*, vol. 26, no. 9, pp. 929–932, May 1, 2014.

[9] Q. Li, Z. Zhang, F. Liu, M. Qiu, and Y. Su, "Dense wavelength conversion and multicasting in a resonance-split silicon microring," *Appl. Phys. Lett.*, vol. 93, no. 8, p. 081113, Aug. 2008.

[10] C. E. Campanella *et al.*, "Localized strain sensing with fiber Bragg-grating ring cavities," *Opt. Exp.*, vol. 21, no. 24, pp. 29435–29441, Dec. 2013.

[11] P. Malara *et al.*, "Split-mode fiber Bragg grating sensor for high-resolution static strain measurements," *Opt. Lett.*, vol. 39, no. 24, pp. 6899–6902, Dec. 2014.

[12] Y. M. Kang, A. Arbabi, and L. L. Goddard, "Engineering the spectral reflectance of microring resonators with integrated reflective elements," *Opt. Exp.*, vol. 18, no. 16, pp. 16813–16825, Aug. 2010.

[13] A. Arbabi, Y. M. Kang, C.-Y. Lu, E. Chow, and L. L. Goddard, "Realization of a narrowband single wavelength microring mirror," *Appl. Phys. Lett.*, vol. 99, no. 9, p. 091105, Aug. 2011.

[14] X. Cai *et al.*, "Integrated compact optical vortex beam emitters," *Science*, vol. 338, no. 6105, pp. 363–366, Oct. 2012.

[15] F. D. Leonardis, C. E. Campanella, B. Troia, A. G. Perri, and V. M. N. Passaro, "Performance of SOI Bragg grating ring resonator for nonlinear sensing applications," *Sensors*, vol. 14, no. 9, pp. 16017–16034, Aug. 2014.

[16] C. E. Campanella, L. Mastronardi, F. D. Leonardis, and V. M. N. Passaro, "Π-shifted fiber Bragg grating ring resonator as a splitting mode resonant sensor," in *Proc. 20th IMEKO TC4 Int. Symp.*, 2014, pp. 414–419.

[17] L. A. Coldren and S. W. Corzine, *Diode Lasers and Photonic Integrated Circuits*. Hoboken, NJ, USA: Wiley, 1995.